Supplementary Information (SI)

Thiol-function UiO-66 anchored atomically dispersed metal ions for photocatalytic selective oxidation of benzyl alcohol

Binbin Guo, [a,b] Rui Chen, [a] Wei Guo, [a] Yueyue Kang, [a] Ling Wu *[a,b]

a: State Key Laboratory of Photocatalysis on Energy and Environment, Fuzhou University, Fuzhou, 350116, China
b: State Key Laboratory of Structural Chemistry, Fujian Institute of Research on the Structure of Matter, Chinese Academy of Sciences, Fuzhou, Fujian 350002, China
E-mail: wuling@fzu.edu.cn

Experimental

Chemicals and materials

Zirconium chloride ($ZrCl_4$, 99%), benzaldehyde (BAD, 98.5%), Chloroauric acid ($HAuCl_4 \cdot 4H_2O$, 99.7%), Chloroplatinic acid ($H_2PtCl_6 \cdot 6H_2O$, 99.7%) and $PdCl_2$ (Palladium chloride, 99.9%) were purchased from Sinopharm Chemical Reagent Co., Ltd. (Shanghai, China). 1,4-benzenedicarboxylic acid (99.0%), Benzyl alcohol (BA, 99%), N, N-Dimethylformamide (DMF, 99.9%), Dichloromethane (99.8%) was purchased from Shanghai Aladdin Bio-Chem Technology Co., Ltd. 2,5-dimercapto-1,4-benzenedicarboxylic acid (H_2MBDC, 98.0%) was purchased from Yanshen Technology Co. Ltd. Benzotrifluoride (BTF, 99%) was purchased from J&K Scientific Ltd. All these chemicals were used as received without further purification.

Synthesis of UiO-66(SH)$_2$

The UiO-66(SH)$_2$ was prepared by a one-step solvothermal reaction as used by Yee et al. [1] 1mmol $ZrCl_4$ and 1mmol 2,5-dimercapto-1,4-benzenedicarboxylic acid were dissolved in 50 mL DMF under vigorous stirring for 30 min. Then, the mixture was transferred into a 100 mL Teflon-lined stainless-steel autoclave, and heated at 120 °C for 24 h. After cooled to room temperature, the yellow precipitate was washed with DMF at 60 °C for 2 hours to remove unreacted substrate. The obtained solid were washed with dichloromethane in the same way as described for the washing with DMF. Finally, the precipitate was washed with ethanol and separated by centrifugation. The collected sample was dried at 60 °C for 24 h.

Synthesis of UiO-66

UiO-66 crystalline powders were prepared according to the procedure for UiO-66(SH)$_2$ by using 1,4-benzenedicarboxylic acid in replace of 2,5-dimercapto-1,4-benzenedicarboxylic acid with all other conditions unchanged.

Synthesis of Pd/UiO-66(SH)$_2$

The Pd nanoparticles was prepared by a reported method. [2] Then 100 mg of the prepared UiO-66 (SH)$_2$ sample was ultrasonically dispersed in 40 mL of ethanol and water mixture (v: v = 1:1) solution. 0.01mmol of Pd nanoparticles was suspended in a 50mL of DI water. The aqueous solution of Pd nanoparticles was injected into the previous step solution of UiO-66 (SH)$_2$. After being constantly stirred for 12 h, the products were collected and washed with water several times, and then dried at 60 °C. The size of Pd nanoparticles was shown in Fig. S22.

Synthesis of UiO-66(SM)$_2$(M=Pd, Pt or Au)

100 mg of the prepared UiO-66 (SH)$_2$ sample was ultrasonically dispersed in 40 mL ethanol and water mixture (v: v = 1:1) solution. 0.01mmol H_2PdCl_4 (10 mg/mL) (or $HAuCl_4$ and H_2PtCl_6) was diluted into a 50mL aqueous solution. Then the aqueous solution of $H_2PdCl_6 \cdot 6H_2O$ was injected into the previous step solution of UiO-66 (SH)$_2$.

After being constant stirred for 12 h, the products were collected and washed with water several times, and then dried at 60 °C.

Characterization

X-ray diffraction (XRD) patterns were performed on a Bruker D8 Advance X-ray diffractometer with Cu Kα radiation (λ = 0.15406 nm) operated at 40 kV and 40 mA to give the phase. Transmission electron microscopy (TEM) image and scanning transmission electron microscopy (STEM) image were collected by using FEI Tecnai G2 F20 field emission transmission electron microscope at an accelerating voltage of 200 kV. The Brunauer-Emmett-Teller (BET) surface area determination was measured on Micromeritics 3500M apparatus. The Fourier transform infrared (FT-IR) spectra of sample was carried out on a Nicolet IS50 Fourier transform infrared spectrometer at a resolution of 4 cm^{-1}. Ultraviolet-visible diffuse reflectance spectra (UV-vis DRS) were obtained *via* an Agilent Cary 500 UV-vis spectrophotometer. Steady state FL spectroscopy and time resolved emission spectroscopy were performed on Edinburgh FLS1000 with Xe lamp and EPL-375 laser source excitation. Inductive Coupled Plasma Emission Spectrometer (ICP) analysis was performed on PerkinElmer Optima 8000. X-ray photoelectron spectroscopy (XPS) analysis and In-situ XPS were measured on an ESCALAB 250Xi photoelectron spectroscopy (Thermo Fisher Scientific Inc.) with monochromatic AlKα Radiation (E =1486.6 eV) and all binding energies were calibrated using C1s at 284.8eV as a reference.

Electrochemistry measurement

The working electrode was prepared on fluorine-doped tin oxide (FTO) glass, which was cleaned by sonicating in ethanol and water for 30 min, respectively. The 5 mg sample was dispersed in 0.5 mL of N, N-dimethylformamide by sonication to get slurry. Then the slurry was spread onto the pre-treated FTO glass. After drying at 393 K for 2 h, a copper wire was connected to the side part of the FTO glass using a conductive tape. The uncoated parts of the electrode were isolated with an epoxy resin and the exposed area of the electrode was 0.38 cm^2. The electrochemical measurements were performed in a conventional three electrode cell, using a Pt plate and a saturated Ag/AgCl electrode as counter electrode and reference electrode, respectively. The working electrode was immersed in a 0.2 M Na_2SO_4 aqueous solution (pH = 6.8) without any additive for 30 s before measurement. The photocurrent measurements were conducted on a CHI660D workstation. A 300 W xenon lamp was used as the visible light source.

Computational Details

The structural and electronic properties of UiO-66(SH)$_2$ were calculated within the framework of density functional theory (DFT) [3, 4] by using the Vienna ab-initio simulation package (VASP) [5-7] with the projector augmented wave (PAW) method.[8] The generalized gradient approximation (GGA) within the Perdew-Burke-Ernzerhof (PBE) type exchange-correlation potentials [9] was used throughout this work. The employed PAW-PBE pseudopotentials [10] of elements Zr, S, O, N, C and H treat $4s^24p^65s^24d^2$, $3s^23p^4$, $2s^22p^4$, $2s^22p^3$, $2s^22p^2$ and $1s^1$ as the valence states, respectively. The plane wave cutoff energy for the expansion of wave functions was set at 600

eV, and the tetrahedron method with Blöchl corrections was used for integrations in the first Brillouin Zone with a k-point mesh, 3 × 3 × 3.

The structure model of UiO-66(SH)$_2$ was built based on the reported cubic crystal structure of UiO-66 by replacing two antithetic H atoms of each benzene ring using the SH groups. By determining the space groups of these structures, a high-throughput screen identified a structure model for UiO-66(SH)$_2$ with the highest symmetry, space group of F*23*, as presented in Table S1 and Fig. S2. By introducing the -SH groups, some S-3p and C-2p orbitals insert into the energy gap of UiO-66, resulting in a smaller bandgap in UiO-66(SH)$_2$, as shown in Fig. S8 and S9.

Photocatalytic activity test

The photocatalytic selective oxidation of BA was performed in a 15 ml quartz tube. In the process, 10 mg of a catalyst, 0.1 mmol of BA, and 1.5 mL of BTF were mixed in the quartz tube. Then the tube was filled with oxygen at a pressure of 1 bar and stirred to make the catalyst blend evenly in the solution. Finally, the suspension was irradiated by a 300 W Xe lamp (Beijing Perfect light Co. Ltd., PLS-SXE300D) with a 420 nm cut-off filter. After 6 h of irradiation, the mixture was centrifuged to completely remove the catalyst particles. The remaining solution was analysed with an Agilent gas chromatograph (GC-7898B). The conversion of BA and the selectivity for BAD were defined as the follows:

Conversion (%) = [(C$_0$ − C$_{BA}$)/C$_0$] × 100%
Selectivity (%) = [C$_{BAD}$/ (C$_0$ − C$_{BA}$)] × 100%

Where C$_0$ is the initial and final concentration of BA and C$_{BA}$ and C$_{BAD}$ are the concentrations of BA and BAD, respectively.
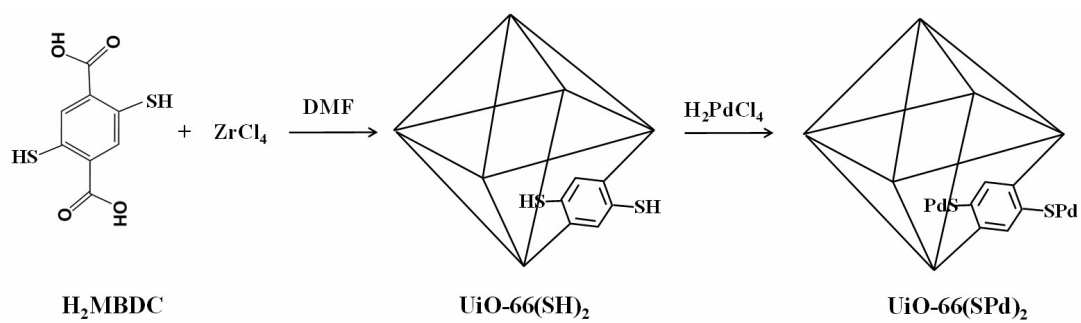
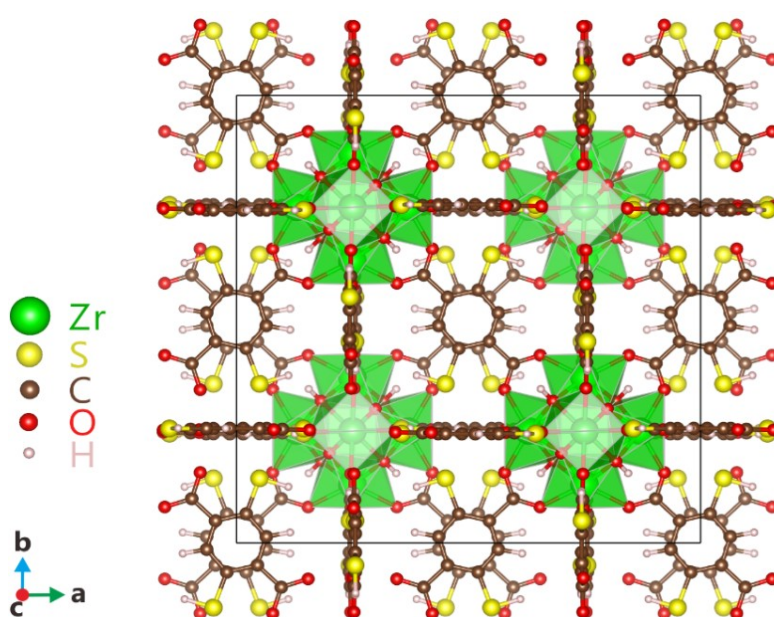**Fig. S1** Synthesis scheme of UiO-66(SH)$_2$ and UiO-66(SPd)$_2$.
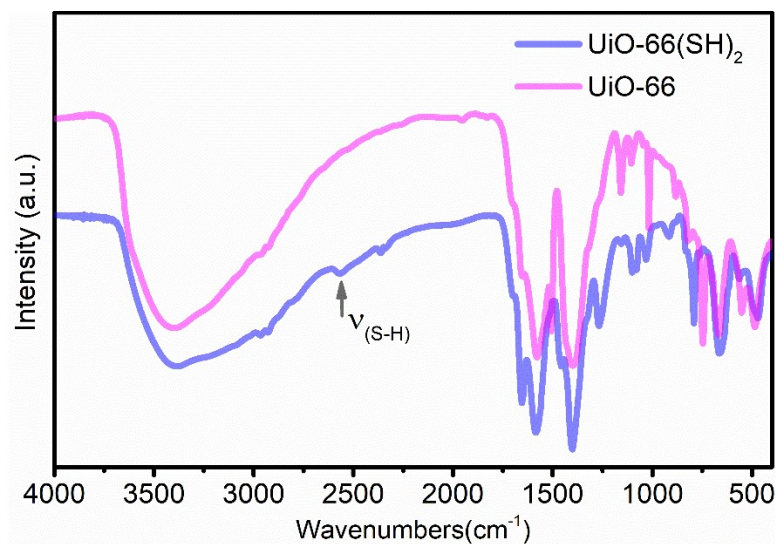

Fig. S2 The crystal structure of UiO-66(SH)$_2$.

Fig. S3 IR spectra of UiO-66 and UiO-66(SH)$_2$.
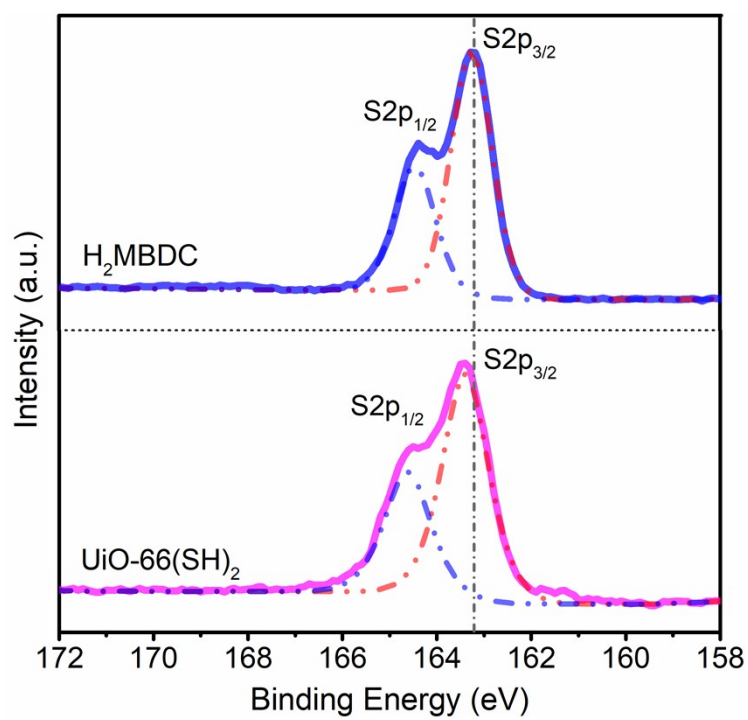

Fig. S4 S 2p XPS spectrum of H$_2$MBDC and UiO-66(SH)$_2$.
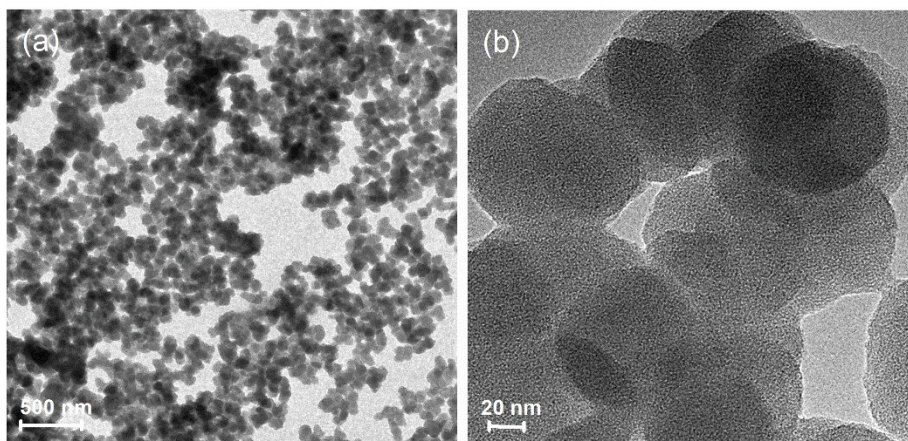
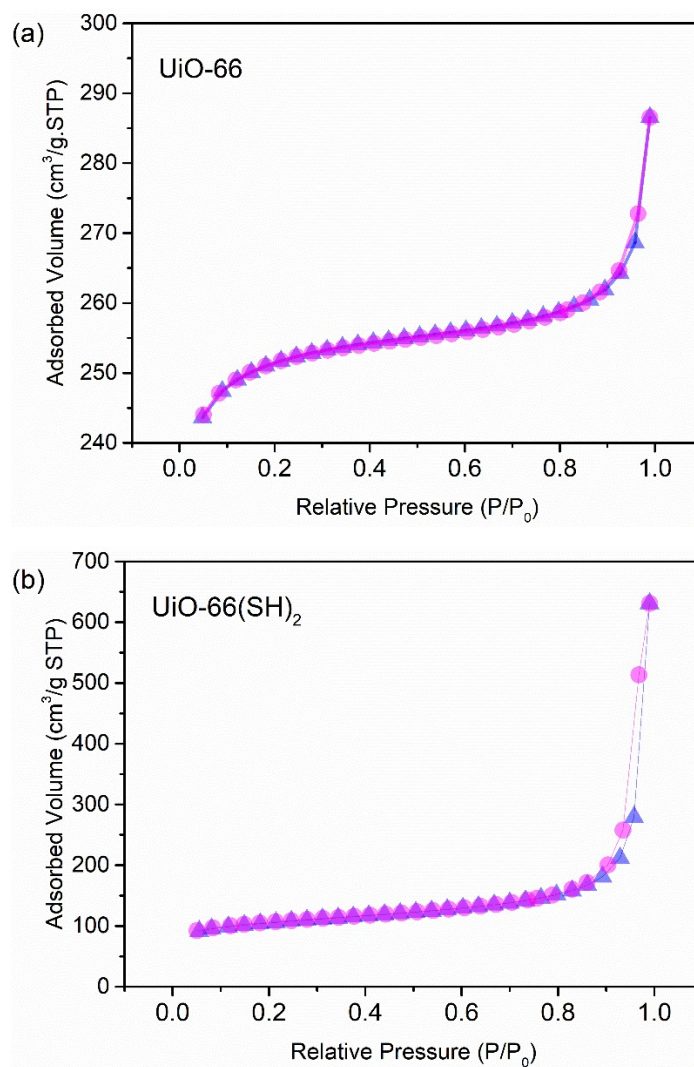**Fig. S5** (a) TEM and (b) HRTEM of the UiO-66(SH)₂.

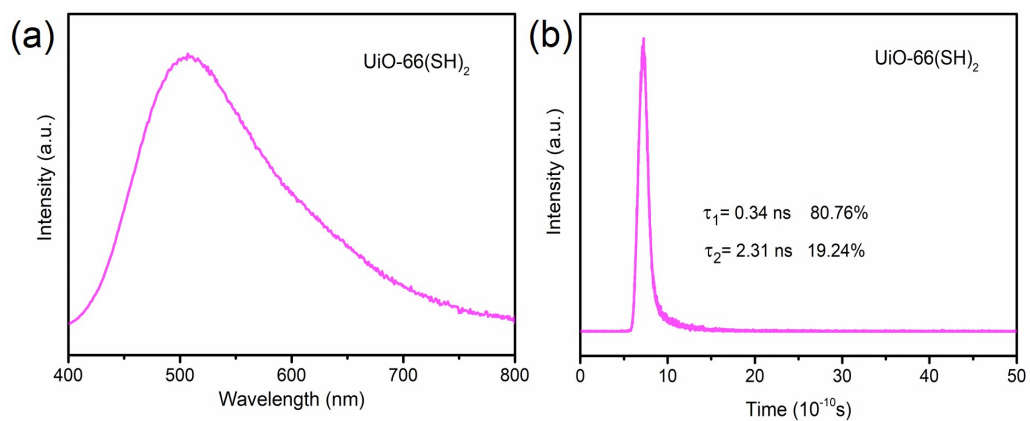**Fig. S6** BET of (a) UiO-66 and (b) UiO-66(SH)₂.

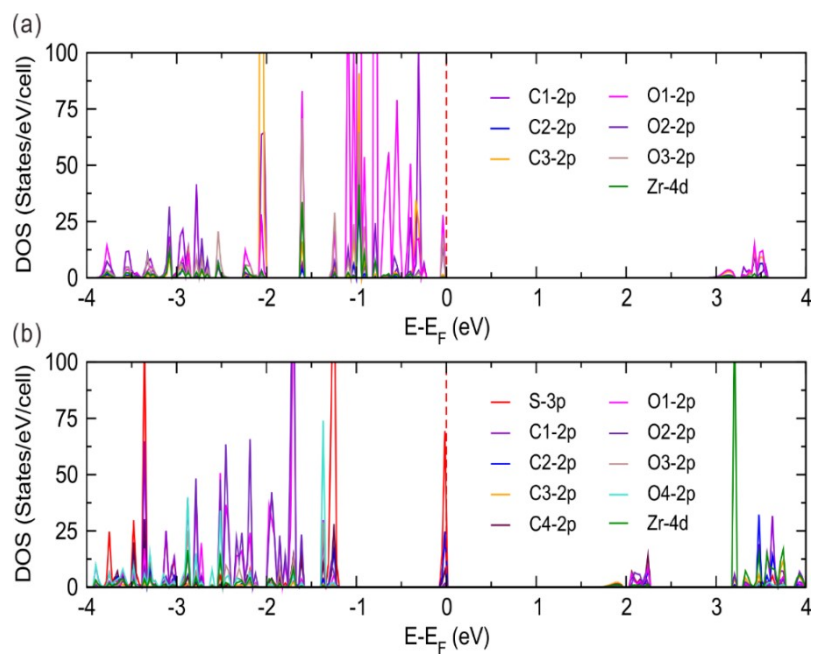**Fig. S7** (a) Room-temperature steady-state PL spectra of the UiO-66(SH)$_2$. (b) The corresponding decay curves of the UiO-66(SH)$_2$.

Fig. S8 Projected density of states (DOS) of (a) UiO-66, and (b) UiO-66(SH)$_2$.
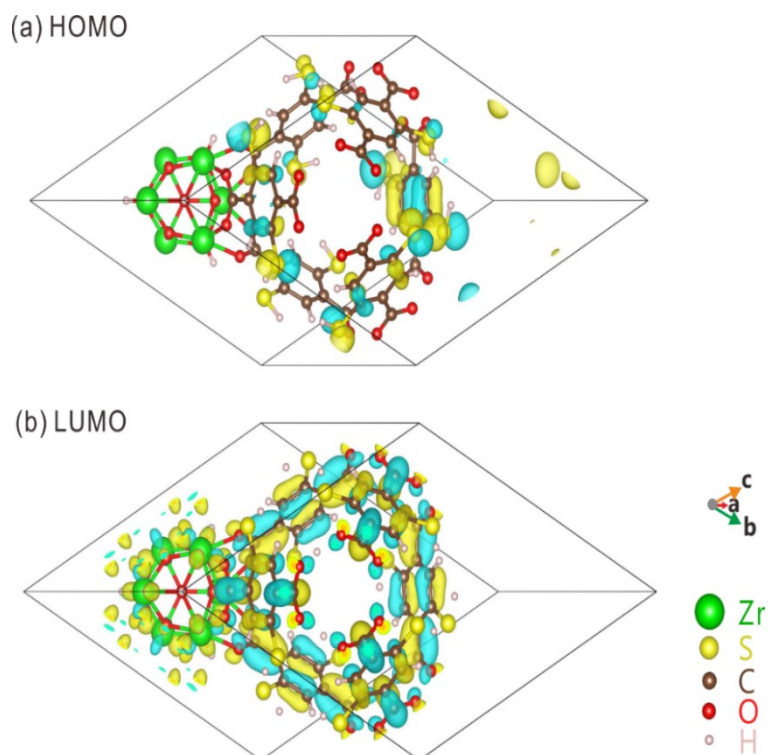
Fig. S9 (a) HOMO band orbital and (b) LUMO band orbital of UiO-66(SH)$_2$ at Γ point.
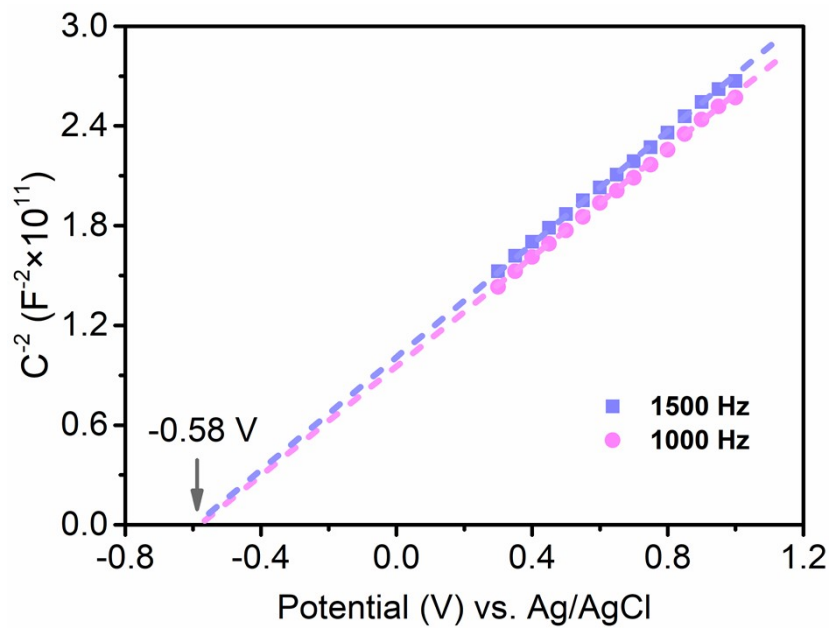
Fig. S10 Mott-Schottky plots of UiO-66(SH)$_2$.
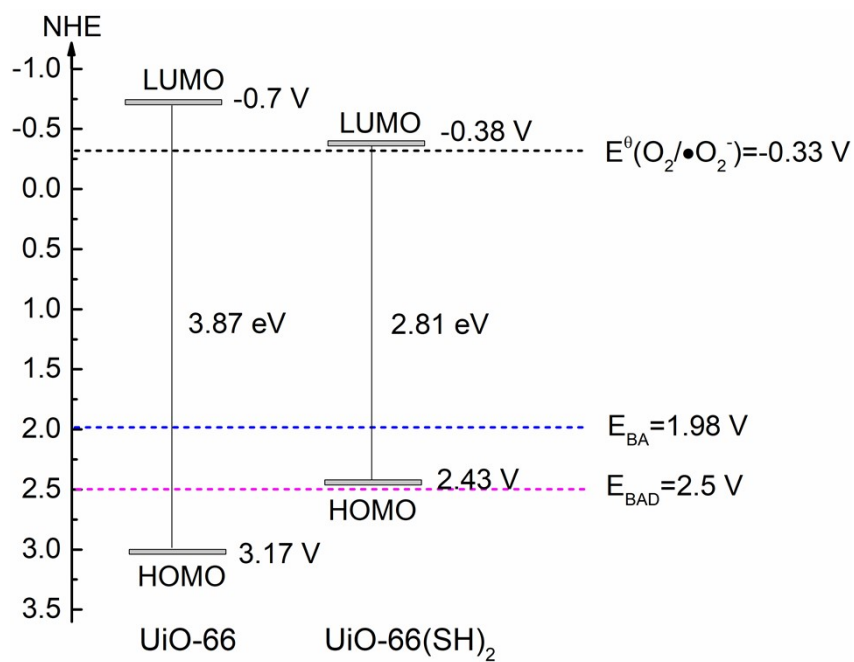
Fig. S11 Energy band positions of UiO-66, UiO-66(SH)$_2$ and the redox potential of BA and BAD.
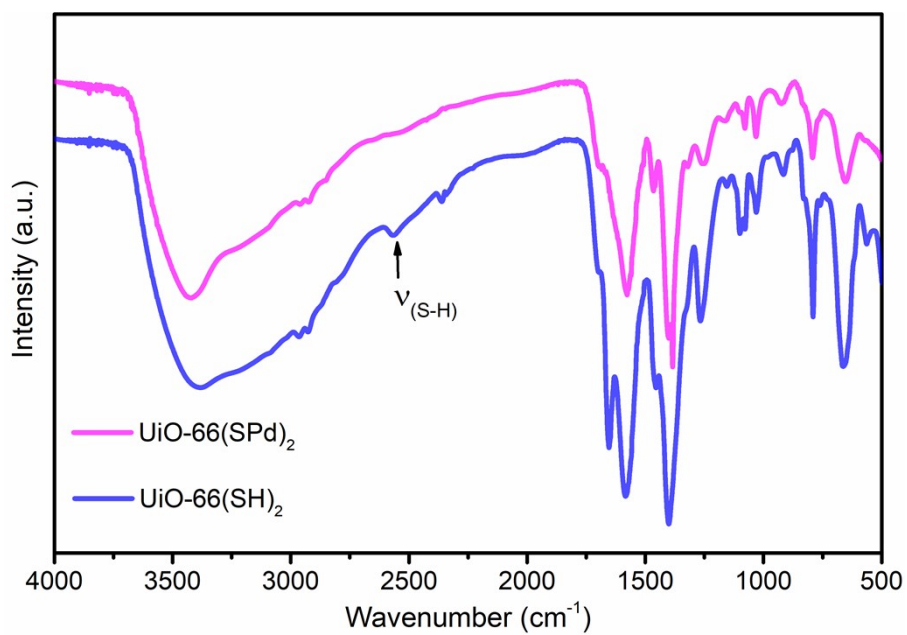
Fig. S12 IR spectra of UiO-66(SPd)$_2$ and UiO-66(SH)$_2$.

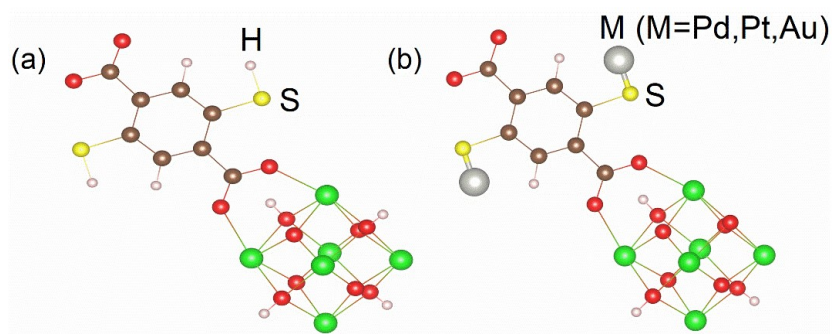**Fig. S13** The coordination model of (a) UiO-66(SH)$_2$, and (b) UiO-66(SM)$_2$(M=Pd, Pt, Au).
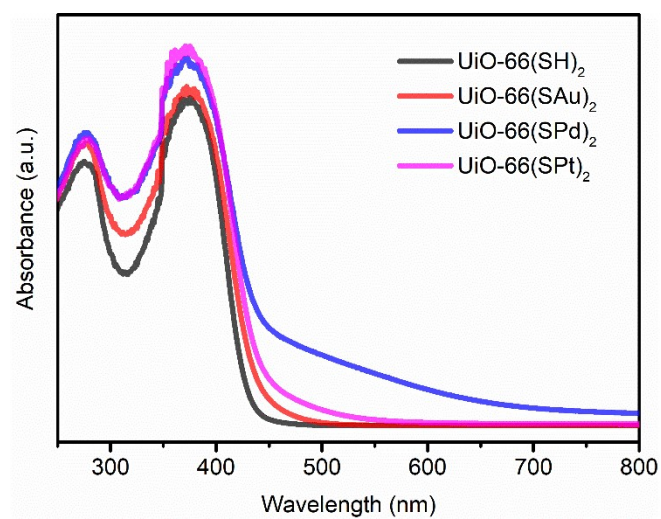

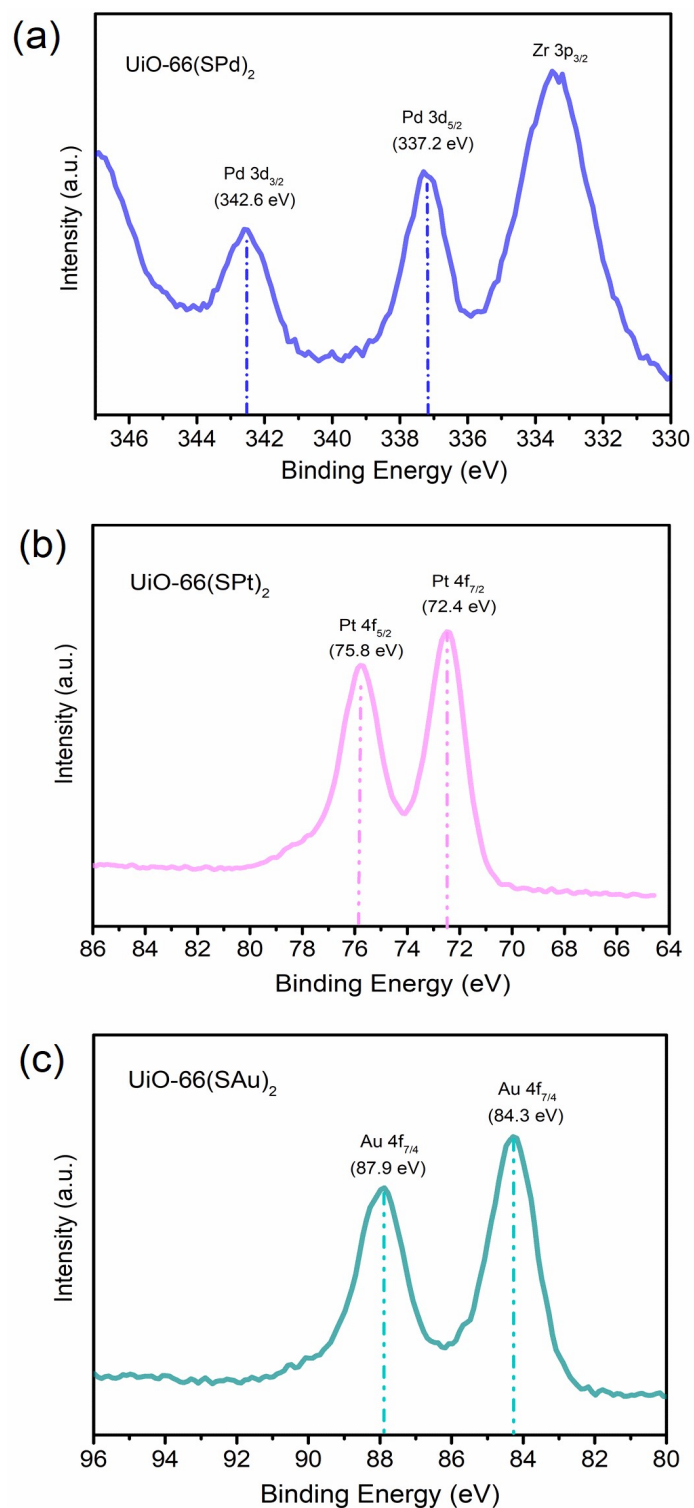Fig. S14 The UV-DRS of UiO-66(SH)$_2$ and UiO-66(SM)$_2$(M=Pd, Pt, Au).

Fig. S15 High resolution XPS spectrum of UiO-66(SM)$_2$(M=Pd, Pt or Au): (a) Pd 3d peaks, (b) Pt 4f peaks, (c) Au 4f peaks.

In this work, H$_2$PdCl$_4$ (or HAuCl$_4$ and H$_2$PtCl$_6$) was used as the precursor, and the valence state of metal ions after anchored was analyzed by XPS. The binding energy of Pd3d$_{5/2}$ located at 337.2 eV, is consistent with Pd(II). It is noteworthy that no signal of Pd metal and Pd(IV)

was detected, if Pd metal is present, the binding energy of Pd 3d should located at 335.3 and 340.6 eV, and if Pd(IV) is present, the binding energy of Pd 3d should located at 338.7 and 344.1 eV. The XPS spectra of Pd $3d_{3/2}$ located at 340.6 eV and 344.1 eV is no signal, the valence state of Pd can be determined to be Pd(II). The binding energy of Pt $4f_{7/2}$ located at 72.4 eV, is consistent with Pt(II). If Pt metal or Pt(IV) is present, the binding energy of Pt $4f_{7/2}$ should located at 71.2 and 74.9 eV. The binding energy of Au $4f_{7/2}$ located at 84.3 eV, is consistent with Au(I). If Au metal or Au(III) is present, the binding energy of Au $4f_{7/2}$ should located at 83.8 and 86.1 eV. [11]
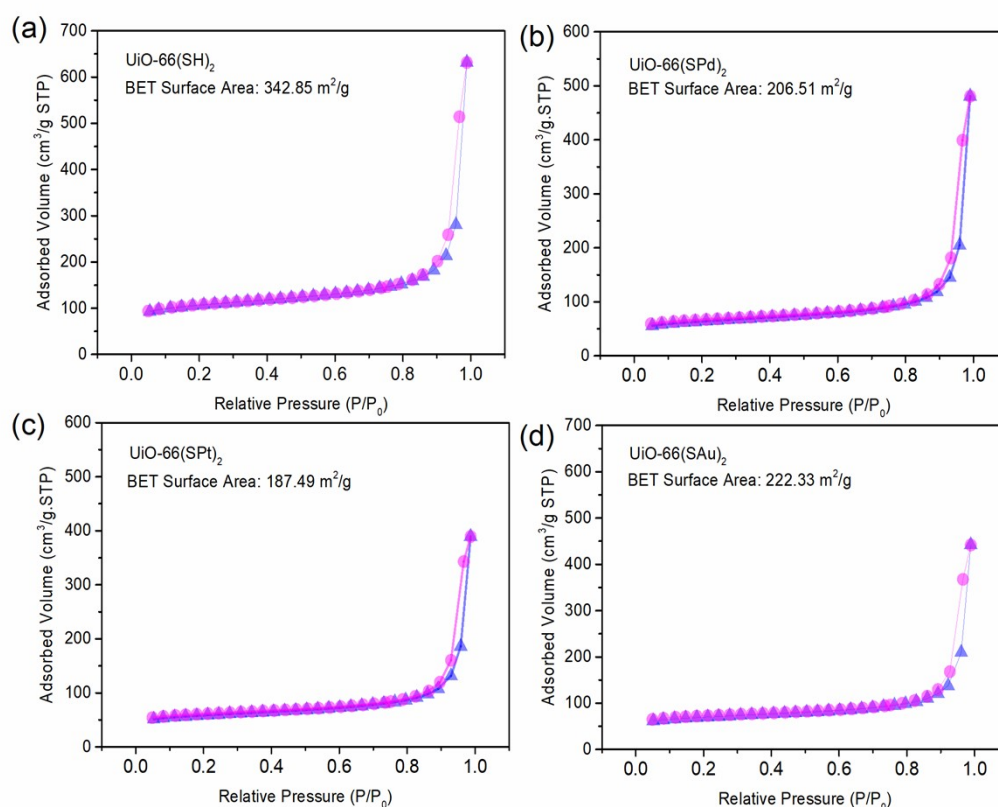

Fig. S16 The BET of (a) UiO-66(SH)$_2$, (b) UiO-66(SPd)$_2$, (c) UiO-66(SPt)$_2$ and (d) UiO-66(SAu)$_2$.
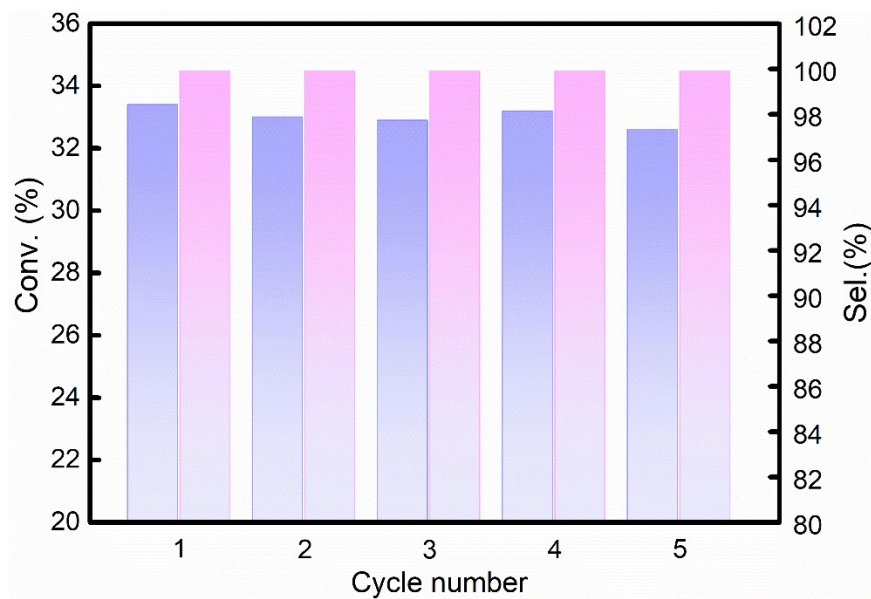
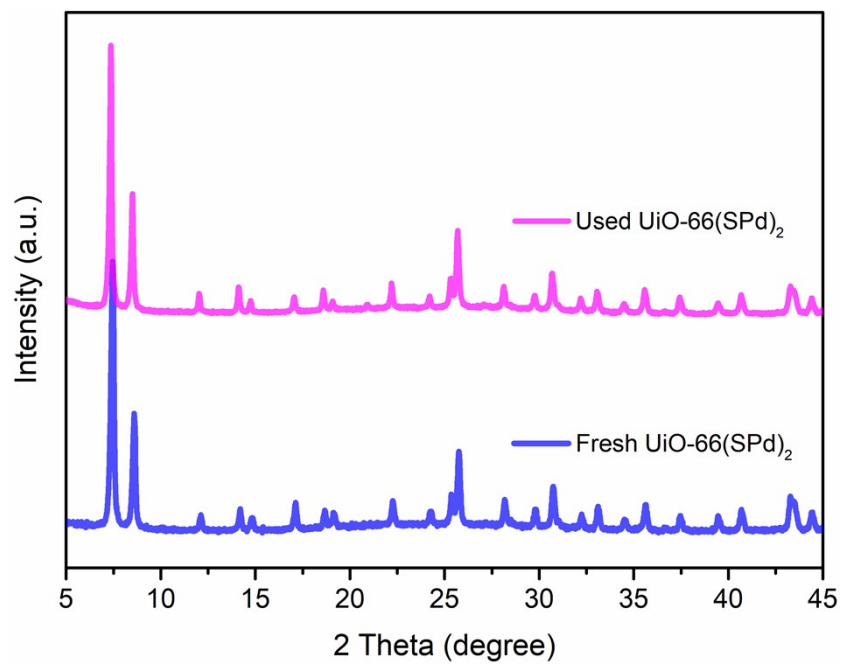**Fig. S17** The recycle experiments for the selective oxidation of BA over UiO-66(SPd)$_2$.

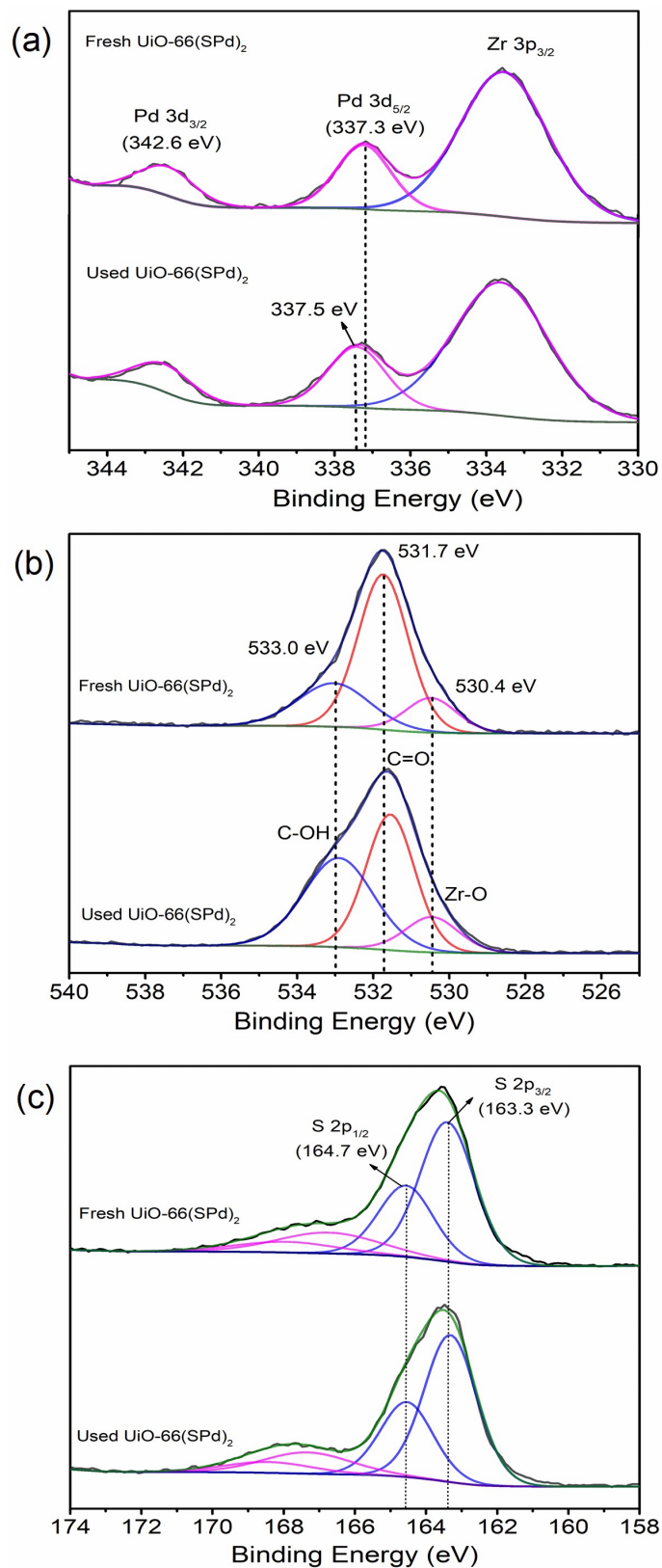**Fig. S18** XRD patterns of fresh UiO-66(SPd)$_2$ and used UiO-66(SH)$_2$.

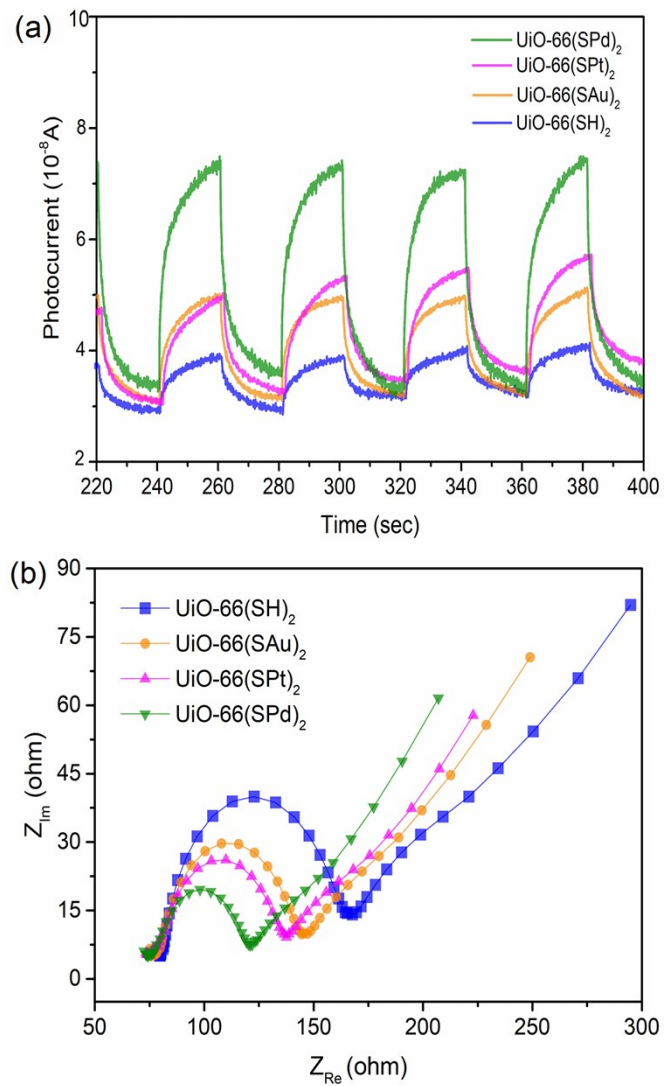**Fig. S19** (a) Pd 3d ; (b) O 1s ; (c) S 2p XPS spectrum of fresh UiO-66(SPd)$_2$ and sued UiO-66(SPd)$_2$.

Fig. S20 (a) Photocurrent response of UiO-66(SH)$_2$ and UiO-66(SM)$_2$(M=Pd, Pt or Au);
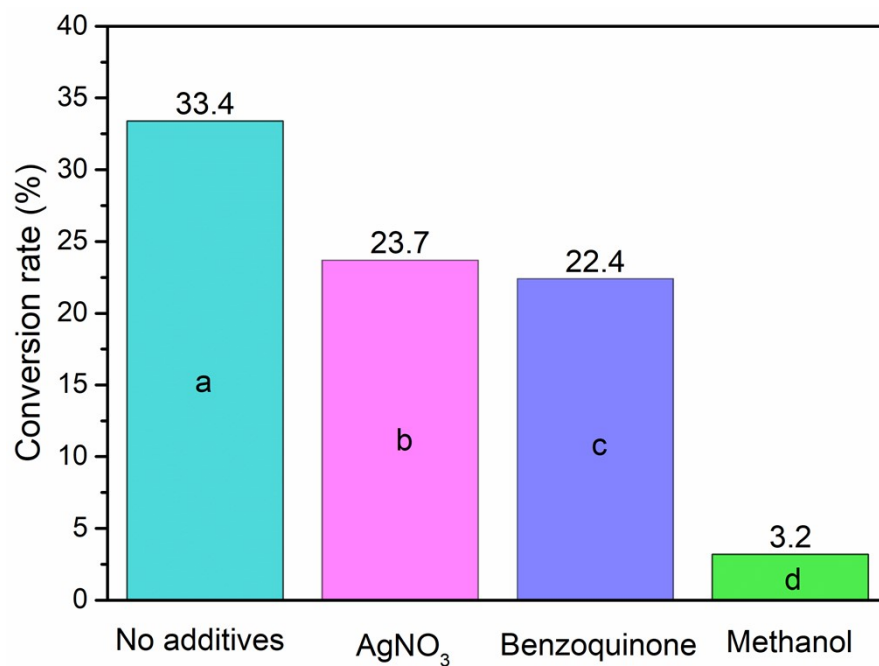(b) electrochemical impedance spectra of UiO-66(SH)$_2$ and UiO-66(SM)$_2$(M=Pd, Pt or Au).

Fig. S21 UiO-66(SPd)$_2$ photocatalytic oxidation of benzyl alcohol at different conditions (a: No additives, b: AgNO$_3$, c: benzoquinone, d: Methanol).
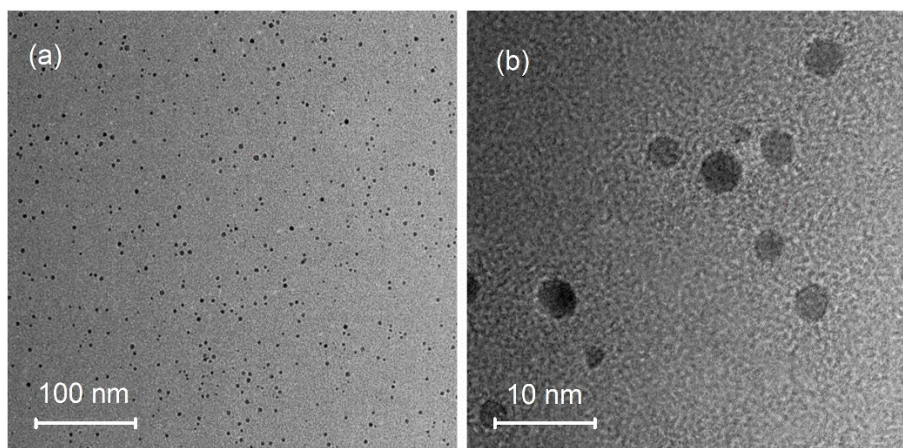

Fig. S22 (a) TEM and (b) HRTEM of the Pd nanoparticles.

Table S1. The crystal structure model of UiO-66(SH)$_2$ (space group: F23) obtained by simulation. The optimized lattice parameter is a = 20.936 Å.

Atom	Wycoff Site	x	y	z
Zr	24g	0.130	0.250	0.250
S	48h	0.144	0.244	0.550
C1	48h	0.065	0.244	0.521
C2	48h	0.064	0.514	0.244
C3	48h	0.096	0.099	0.254
C4	48h	0.045	0.050	0.256
O1	48h	0.078	0.157	0.253
O2	48h	0.080	0.253	0.154
O3	16e	0.183	0.183	0.183
O4	16e	0.300	0.300	0.300
H1	48h	0.126	0.243	0.612
H2	48h	0.116	0.523	0.244
H3	16e	0.156	0.156	0.156

Table S2. The content of anchor Au, Pd and Pt on UiO-66(SM)$_2$. [a]

Sample	Element	Concentration (mg/L)	Weight%
UiO-66(SAu)$_2$	Au	8.31	1.66
UiO-66(SPd)$_2$	Pd	8.81	1.76
UiO-66(SPt)$_2$	Pt	8.66	1.73

[a] 5 mg UiO-66(SM)$_2$ sample was dissolved in 3 mL HNO$_3$ (65%), and then transferred to a 10 mL volumetric flask with deionized water for constant volume, and the test was carried out after the mixture was evenly mixed.

References

1. K. K. Yee, N. Reimer, J. Liu, S. Y. Cheng, S. M. Yiu, J. Weber, N. Stock and Z. Xu, *J. Am. Chem. Soc.*, 2013, **135**, 7795-7798.
2. D. Shuai, D. C. McCalman, J. K. Choe, J. R. Shapley, W. F. Schneider and C. J. Werth, *ACS Catal.*, 2013, **3**, 453-463.
3. P. Hohenberg and W. Kohn, *Phys. Rev. B*, 1964, **136**, B864.
4. W. Kohn and L. J. Sham, *Phys. Rev.*, 1965, **140**, A1133.
5. G. Kresse and J. Hafner, *Phys. Rev. B*, 1993, **47**, 558-561.
6. G. Kresse and J. Furthmuller, *Comput. Mater. Sci.*, 1996, **6**, 15-50.
7. G. Kresse and J. Furthmuller, *Phys. Rev. B*, 1996, **54**, 11169-11186.
8. P. E. Blochl, *Phys. Rev. B* 1994, **50**, 17953-17979.
9. J. P. Perdew, K. Burke and M. Ernzerhof, *Phys. Rev. Lett.*, 1996, **77**, 3865-3868.
10. J. P. Perdew and Y. Wang, *Phys. Rev. B*, 1992, **45**, 13244-13249.
11. M. C. Bourg, A. Badia and R. B. Lennox, *J. Phys. Chem. B*, 2000, **104**, 6562-6567.